Langmuir

Article

pubs.acs.org/Langmuir

Rod Packing in Chiral Nematic Cellulose Nanocrystal Dispersions Studied by Small-Angle X-ray Scattering and Laser Diffraction

Christina Schütz,[†,‡] Michael Agthe,[†] Andreas B. Fall,[†] Korneliya Gordeyeva,[†] Valentina Guccini,[†,‡] Michaela Salajková,[§] Tomás S. Plivelic,[∥] Jan P. F. Lagerwall,[⊥] German Salazar-Alvarez,[†,‡] and Lennart Bergström*[,†]

[†]Department of Materials and Environmental Chemistry, Stockholm University, 106 91 Stockholm, Sweden

[‡]Wallenberg Wood Science Center, KTH, 100 44 Stockholm Sweden

[§]Department of Biosciences, University of Oslo, 0371, Oslo, Norway

[∥]MAX IV Laboratory, Lund University, PO Box 118, 221 00 Lund, Sweden

[⊥]Physics and Materials Science Research Unit, University of Luxembourg, Luxembourg City 1511, Luxembourg

Supporting Information

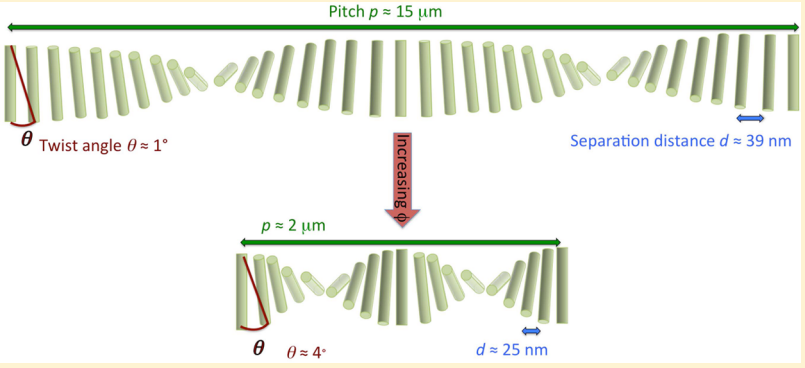

ABSTRACT: The packing of cellulose nanocrystals (CNC) in the anisotropic chiral nematic phase has been investigated over a wide concentration range by small-angle X-ray scattering (SAXS) and laser diffraction. The average separation distance between the CNCs and the average pitch of the chiral nematic phase have been determined over the entire isotropic−anisotropic biphasic region. The average separation distances range from 51 nm, at the onset of the anisotropic phase formation, to 25 nm above 6 vol % (fully liquid crystalline phase) whereas the average pitch varies from ≈15 μm down to ≈2 μm as ϕ increases from 2.5 up to 6.5 vol %. Using the cholesteric order, we determine that the twist angle between neighboring CNCs increases from about 1° up to 4° as ϕ increases from 2.5 up to 6.5 vol %. The dependence of the twisting on the volume fraction was related to the increase in the magnitude of the repulsive interactions between the charged rods as the average separation distance decreases.

INTRODUCTION

Biopolymers, like DNA, peptides, and polysaccharides, are well-known to form liquid crystalline phases, primarily with a nematic or chiral nematic structure.[1] These structures are important for the biological and mechanical function. Indeed, the importance of a helical arrangement of rod-like polysaccharide crystals for the mechanical strength of biomineralized composites was already recognized by Bouligand,[2] and recent work has related the high fracture resistance of the dactyl club of a stromatopod[3] and the cuticle of lobster[4] to the helical structure of mineralized chitin fibrils.

Cellulose, the most available polymer in nature, has the ability to form helical structures, both in plants and in aqueous dispersions of cellulose nanocrystals (CNC).[5,6] Dispersions of colloidally stable CNC can form a chiral nematic (N*) liquid crystalline phase (a rare case of rejection of this well-established interpretation is discussed in the Supporting Information).

It has been shown that the phase behavior depends on the aspect ratio,[7,8] the surface chemistry of the CNC rods,[9] and also the ionic strength of the aqueous medium.[10−12] The polydisperse CNC particles are commonly approximated by a rod-like geometry with diameters around 5 nm and lengths varying from 100 to 500 nm although the cross section are actually rectangular.[13] The helical arrangement within CNC dispersions has recently attracted a significant interest for templating chiral inorganic, carbon materials, and polymers with useful optical and mechanical properties.[14−17]

The pitch of the chiral nematic phase, i.e., the periodicity of the helical modulation at the direction along which the CNC align locally, is usually characterized by polarized optical

Received: March 12, 2015
Revised: May 28, 2015
Published: May 28, 2015

DOI: 10.1021/acs.langmuir.5b00924
Langmuir 2015, 31, 6507−6513

microscopy.[18] Pitch values ranging between 10 to 60 μm have been found in previous studies,[8,10−12,19] but little is known on how the pitch varies with volume fraction. The structural features of the chiral nematic CNC phase have been investigated to some extent by small-angle X-ray and neutron scattering (SAXS and SANS).[20−22] SANS[20] was e.g. used to show that the CNC rods in magnetically and shear aligned chiral nematic CNC dispersions are more tightly packed along the chiral nematic axis than perpendicular to it. Orts et al.[20] also showed that the rod spacing decreases with increasing CNC concentration and added electrolyte content. However, the equilibrium rod packing and specifically the spacing and the pitch of CNC dispersions, or the twist angle between interacting CNC rods, have not been investigated previously.

In the present work, we have studied the structural features on two different length scales of the chiral nematic phase formed by cellulose nanocrystals. We have analyzed the separation distances between the CNC rods by SAXS and determined the size of the pitch in the chiral nematic phase by laser diffraction. The twist angle between neighboring CNC rods was then calculated over a wide concentration range and related to pair-potential estimates for different orientations of interacting CNC rods.

EXPERIMENTAL SECTION

Preparation of Cellulose Nanocrystals (CNC). Cellulose nanocrystals (CNC) were prepared by sulfuric acid hydrolysis of Domsjö dissolving wood pulp (60/40 spruce/pine, 95% cellulose, 4.5% hemicellulose, and 0.3% lignin). 20 g of wood pulp was dispersed in 175 mL of 64% sulfuric acid at 45 °C for 40 min. The reaction was quenched by dilution with a 10-fold amount of deionized water. The resulting dispersion was washed by centrifugation at 6000 rpm for 10 min (Hettich EBA 21) twice. The purified CNC was collected and dialyzed with deionized water at a steady flow of 36 L/h in a 4 L container for 5 days, using dialysis membranes with a molecular weight cutoff of ∼14 000 Da (Sigma-Aldrich). After the dialysis the dispersion was sonicated for 10 min with an ultrasonic probe at 70% energy output (Sonics Vibracell VC-750, USA), using a 13 mm wide titanium probe, and centrifuged to retrieve the CNC. The CNC concentration in the dispersions was increased by controlled evaporation at room temperature. The solid content of CNC in the aqueous dispersion was determined by gravimetry with a relative error of 2%, and the volume fraction of CNC was calculated by using a density for cellulose of 1.6 g/cm^3.[23] The sulfate half-ester provided the CNCs with a surface charge of 0.23 mmol/g CNC, as determined by polyelectrolyte titration.

Determination of Volume Fraction of the Liquid Crystalline Phase. The CNC dispersions with volume fractions were filled into glass vials with a diameter of 1 cm and a total volume of approximately 4 mL and equilibrated at room temperature in sealed vials for up to 6 months. The vials were imaged with a Fujifilm Finepix F200 EXR camera (f = 6.4 mm, F3.3, ISO-100, 1/6 s exposure time) between crossed polarizers. The images were analyzed using ImageJ[24] to determine the ratio between the total height of the dispersion and the height of the anisotropic phase. The accuracy of the determination of the volume fraction of the liquid crystalline phase has a relative error less than 10%.

Small-Angle X-ray Scattering. Small-angle X-ray scattering (SAXS) experiments were performed at the beamline I911-4 at MAX-lab, Lund, Sweden.[25] The beamline uses a multipole wiggler where the Si(111) monochromator provides a photon flux of 5 × 10^{10}/s in 0.2 × 0.3 mm^2 with a wavelength of 0.91 Å. The sample−detector distance was 2341.5 mm (q-range 0.07 ≤ q ≤ 3.5 nm^{-1}), and typical exposure times ranged between 100 and 600 s. The CNC dispersions were filled into borosilicate capillaries with a diameter of 2 mm with a 10 μm wall thickness (Hilgenberg GmbH, Germany) at least 10 h prior to measurement. The 2D SAXS data were obtained using a hybrid pixel X-ray detector (Pilatus 1M, Dectris). The background scattering of pure water and the capillary was subtracted prior to radial integration with the bli9114 (version 4.71) software[25] and subsequently analyzed using SasView 3.0.[26] The observed intensities were Lorentz-corrected, and the goodness of fit expressed in terms of the adjusted R-square value of the Gaussian function was always better than 0.999.

Determination of the Pitch of CNC Dispersions with Laser Diffraction. The laser diffraction measurement setup consisted of capturing the scattering pattern onto a white screen by a digital camera (Fujifilm Finepix F200 EXR, f = 6.4 mm, F3.3, ISO-100, 1−5 s exposure time). The scattering pattern is created by illumination of the CNC dispersions by an ordinary pen-shaped laser (λ = 522−542 nm, beam diameter 1.2 mm). The distance between the screen and the different components were fixed at 395 mm (sample to screen), 542 mm (laser to screen), and 550 mm (camera to screen). The obtained diffraction patterns were analyzed by radial integration using ImageJ[24] (1.48, with plugin radial profile extended by Philippe Carl). The resulting curves were analyzed using Origin 8.5 fitting the background and the peaks with a polynomial of the fourth order and a Gaussian function, respectively. The CNC dispersions were filled in glass vials and equilibrated between 38 h and 6 months prior to measurement.

Polarized Optical Microscopy. The polarized optical microscopy (POM) images were taken in reflection mode on a Nikon Eclipse FN1 light microscope (Nikon, Japan) equipped with a 10× eyepiece and a 10× objective (WD 17.5 mm, NA 0.30) between crossed polarizers. The photos were recorded using an inline camera with a 2 megapixel CCD sensor (Kappa Zelos-02150C GV, Kappa Optronics GmbH, Germany). The pitch values were extracted by analyzing Fourier transforms (FFT) of the POM images using ImageJ[24] (version 1.48v, results in Supporting Information Table S1). The CNC dispersions were placed in 3.3 cm long capillaries with a rectangular cross section 0.20 × 4.0 mm^2 (Vitrotubes). The capillaries were sealed with epoxy resin and stored at room temperature for at least 1 week before imaging.

Scanning Transmission Electron Microscopy. The scanning transmission electron microscope (STEM) images of CNC were obtained using a JSM-7401F microscope in STEM mode. An accelerating voltage of 20 kV was used with a working distance of 6 mm. The specimens were prepared by depositing a 6.3 × 10^{-5} vol % dispersion on a holey carbon grid (01824 AC-U on Holey, 400 Mesh Cu, Ted Pella). After 2 min the remaining dispersion was removed by filter paper and the grid was dried at room temperature for 1 h. The length of 200 CNC particles was manually measured, and the mean length and its standard deviation were determined (see Supporting Information Figure S3).

Atomic Force Microscopy. A drop (10 μL) of pure (3-aminopropyl)triethoxysilane (APTES) solution was deposited on a freshly cleaved mica surface, allowed to react for 30 s, and then blow-dried with compressed air. A droplet of CNC dispersion (6.3 × 10^{-3} vol %) was deposited on the treated surface for 30 s and dried with compressed air.

The used cantilevers were MPP-11100-10 from Veeco with a force constant of 20−80 N/m. The AFM measurements were carried out in tapping mode using Dimension 3100 SPM with a NS-IV controller, Veeco, USA, instrument. The force was kept minimal during scanning by routinely decreasing it until the tip detached from the surface and subsequently increasing it slightly to regain contact. The recording scan rate was set between 0.5 and 2 lines/s. The images of 512 × 512 px^2 were analyzed with the noncommercial software WSxM 5.0 Develop 1.3.[27] The length of 200 CNC particles were manually measured, and the mean length and its standard deviation were determined by fitting the corresponding histogram (see Supporting Information Figure S1). The width was determined using MatLab and the toolbox DIPimage. Several thousands of particle height values were collected per sample, including several data points per particle, and discarding regions close to particle−particle overlap (results Figure S2).

Calculation of Pair Potentials. The pair potential of two interacting CNC rods was determined by summation of the

DOI: 10.1021/acs.langmuir.5b00924
Langmuir 2015, 31, 6507−6513

electrostatic repulsion and the van der Waals attraction according to the DLVO framework[28,29] for parallel and crossed solid cylinder arrangements.[30−32] The Hamaker constant for cellulose−water−cellulose, 8 zJ, was taken from Bergström et al.[33] The electrostatic calculations were performed at constant surface charge, where the surface charge density was estimated assuming a diameter of the CNC rods of 4 nm. The Graham equation was used to relate the surface potential, ψ_s, to the surface charge density.[30] The effective surface charge density of nanocellulose was assumed to be significantly reduced due to counterion adsorption;[34] we have inferred a reduction of 80% of the experimentally determined surface charge density (−35 mC/m^2) based on previous estimates by Israelachvili for rod-shaped particles.[30]

RESULTS AND DISCUSSION

The CNC dispersions investigated in this study form an anisotropic phase at CNC volume fractions approximately above 1.9 vol %, as shown in Figure 1. Figure 1a shows that the relative volume of the lower anisotropic phase; i.e., the left-handed chiral nematic (N*) liquid crystalline phase increases as the total CNC concentration increases, and the dispersion is fully anisotropic at volume fraction $\phi \approx 4.5$ vol % after 91 h.

The phase separation process is time dependent, and it takes several days for the dispersion to equilibrate. This is illustrated by the turbidity observed in the upper isotropic phase of the dispersions in Figure 1a and the time-dependent phase diagram in Figure 1b. As shown in Figure 1b, full liquid crystallinity, represented by $\phi_{LC} = 1$ appears to be reached at above approximately 4.2 vol % after 40 h, but with increasing equilibration time this shifts to ca. 5.2 vol % after 6 months. This suggests that small-scale isotropic domains initially exist in the slightly lower concentrated samples, but distributed within a continuum of liquid crystalline phase in such a way that they initially cannot be detected as they slowly sediment. Another possibility is that the CNC particles are slowly loosing surface charge with time.[35]

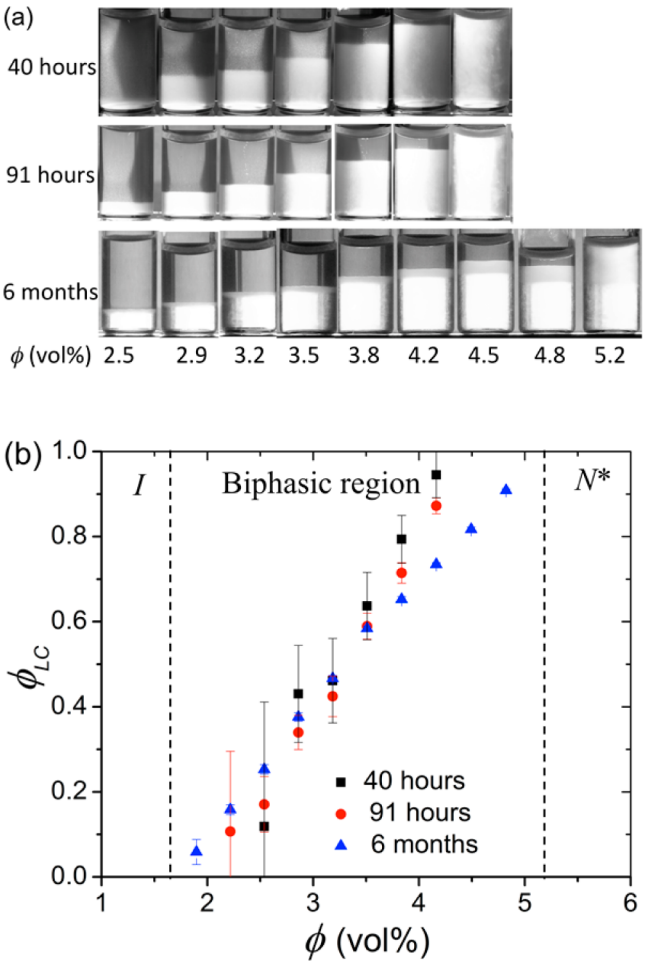

Figure 1. Phase behavior of aqueous dispersions of cellulose nanocrystals (CNC) after 40 h, 91 h, and 6 months equilibration. (a) Photographs of phase-separated CNC dispersions acquired between crossed polarizers. (b) Volume fraction of liquid crystalline phase ϕ_{LC} as a function of the total volume fraction of the CNC ϕ.

The length and aspect ratios for the CNC investigated in this study have been evaluated by several different methods. Size analysis of CNC deposited on a positively charged mica substrate from atomic force microscopy (AFM) tapping mode images gives an average length of $\langle L \rangle = 178$ nm with $\sigma = 76$ nm and an average width $\langle D \rangle = 5.2$ nm with $\sigma = 2.0$ nm (for details see Figures S1 and S2), corresponding to an aspect ratio L/D of 34. Analysis of scanning transmission electron microscopy (STEM) micrographs reveals an average length $\langle L \rangle = 131$ nm with $\sigma = 68$ nm (Figure S3). The dimensions of the CNCs were also determined by small-angle X-ray scattering measurements of diluted CNC dispersions (see Supporting Information for details). The best fit to the data was obtained by using a rectangular prism model with dimensions of the short sides $\langle a \rangle \times \langle b \rangle = 1.6 \times 6.4$ nm^2 with $\sigma = 1.0 \times 3.2$ nm^2 and the long side $\langle L \rangle = 237$ nm with $\sigma = 107$ nm. However, the simplified cylindrical rod model with a polydisperse cylindrical form factor[36,37] with average diameter $\langle D \rangle = 4.0$ nm and $\sigma = 2.4$ nm also gives a good fit to the data (see Figure S4 in the Supporting Information for details). The significant differences in average length of the CNC as determined by AFM and STEM can be attributed to the large polydispersity, differences in deposition procedure, and the limited number of measured CNC particles (200 measured particles for AFM and STEM). The slightly larger measured diameter using AFM (5.2 nm) compared to the diameter determined by SAXS (4.0 nm, assuming a cylindrical rod geometry) can be related to the inability to accurately determine the dimensions of materials with a high curvature by AFM. Thus, the aspect ratio depends on the method(s) used to characterize the dimensions of the CNC, which yields values ranging from 25 to 59. Using a mean value of the average rod lengths determined by AFM and STEM, $\langle L \rangle = 154$ nm, and the average diameter determined by SAXS, an average aspect ratio of 38 is obtained.

Figure 2a shows the Lorentz-corrected small-angle X-ray scattering curves of CNC dispersions at different volume fractions. All of them display two peaks where the peak positions move to higher q values (shorter distances) with increasing CNC concentration, and the peak at higher q values diminishes in intensity. We have estimated the average correlation distance d of the N* phase by fitting a Gaussian function to the primary peak of the Lorentz-corrected SAXS curves shown in Figure 2a. Figure 2b shows that d decreases with increasing CNC content; from about 51.0 nm at $\phi = 1.3$ vol % down to a spacing of 24.5 nm at $\phi = 6.5$ vol %. It is worth mentioning that the determined distances, d, are several times the width of a CNC particle, suggesting that the polydispersity of the particles does not play an important role in the packing of the rods at the investigated concentration range.

As depicted in the insets of Figures 2b and 3, the rods in a chiral nematic phase organize without lateral positional

DOI: 10.1021/acs.langmuir.5b00924
Langmuir 2015, 31, 6507−6513

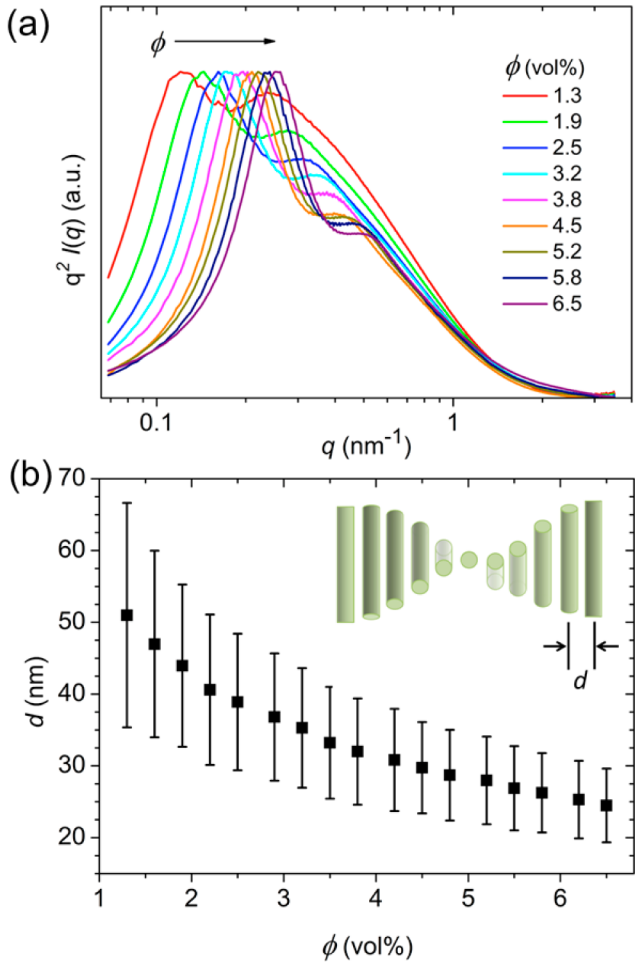

Figure 2. Small-angle X-ray scattering (SAXS) and average separation distances of CNC dispersions: (a) Lorentz-corrected intensities ($I \times q^2$) against the scattering vector q of CNC dispersions with volume fractions ϕ ranging from 1.3 to 6.5 vol %. (b) Average center-to-center separation distance (d) as a function of volume fraction ϕ. The error bars represent the standard deviation of the fitted Gaussian peaks. The inset shows a schematic representation of the helical arrangement of the CNC rods indicating the separation distance between two neighboring rods.

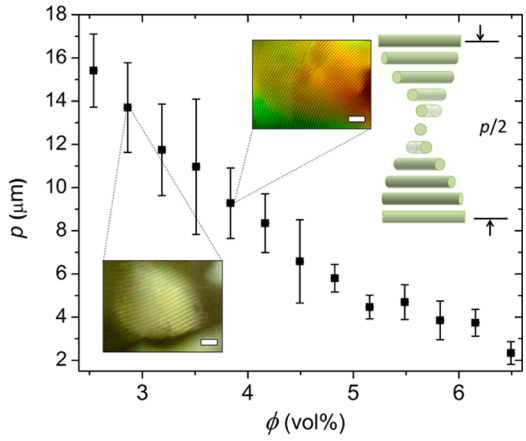

Figure 3. Helical pitch (p) as a function of CNC volume fraction (ϕ) determined by laser diffraction. The symbols represent the experimental values and the error bars the standard deviation σ from Gaussian peak fits. The top-right inset includes a schematic representation of the helically arranged CNC rods where the length of $p/2$ is indicated by the two arrows. Other insets correspond to POM images of samples at 2.9 vol % (p = 13.7 μm) and 3.8 vol % (p = 9.3 μm); the scale bar in the insets represents 20 μm.

ordering but with a director rotating in a helical fashion orthogonal to the rod's long axis.[38] The pitch, p, defined as the period of this variation, has been determined by polarized optical microscopy (POM).[8,10,12,39] The POM images in the insets of Figure 3 for CNC dispersions at volume fractions within the biphasic region clearly show domains with distinct and regularly spaced extinction lines. The fast Fourier transform (FFT) of the POM images reveal that the distances between the extinction lines ($p/2$), and thus the pitch, decrease with increasing ϕ (Supporting Information, Table S1). However, since POM provides useful information only at local level and only when the director lies parallel to the glass slide, we used laser diffraction (see Figure S6 for an illustration of the setup) to obtain information over a much larger volume. We were able to obtain distinct laser diffraction patterns at CNC volume fractions above 2.5 vol %, where the dispersions contain a significant amount of the chiral nematic phase.

Figure 3 (and column 5 of Table S1) shows that the pitch decreases from ≈15.4 μm down to ≈2.3 μm as ϕ increases from 2.5 up to 6.5 vol %. The pitch appears to level off at high CNC concentrations, in accordance with theoretical calculations by Wensink and Jackson.[40] Beck-Candanedo et al.[7] also observed a decrease in pitch with increasing CNC content. Quantitatively, however, they found considerably longer pitch values than those in our study, suggesting a pitch range from ca. 20 to ca 10 μm as the CNC content increases from 7 to 13 wt % (i.e., ≈4.5 to ≈8.5 vol %). Specifically, they report a pitch of 18 μm for a 7 wt % CNC dispersion, a concentration for which we find p more than half the size (6.6 μm). Both systems have nearly the same surface charge density. Theoretical predictions[41] and studies of rod-like virus filamentous bacteriophage fd viruses[42] suggest that the magnitude of the pitch should scale with the inverse of the aspect ratio, $p \propto D/L$. Although the difference in measured pitch between our system and Beck-Candanedo et al.[7] seems to follow this relation (average aspect ratios 38 and 30, respectively), the difference in pitch is probably too large to be explained solely by this structural difference.

The SAXS and laser diffraction measurements yield information on how the average distances between the CNCs and the pitch values vary with ϕ. We have used these values to calculate the angle (θ) one rod has to twist in relation to its neighbor assuming that $\theta(\phi) = 360° \; d(\phi)/p(\phi)$. Figure 4 shows that θ increases from about 0.9° up to about 3.7° as ϕ increases from 2.5 to 6.5 vol %.

The origin of the twist in chiral nematic phases is a debated issue[43] and often related to a competition between entropic and enthalpic contributions to the total energy of the system. The enthalpic contributions that stem mainly from the rod−rod interactions become important when the separation distances between the rods is relatively small, i.e., at high CNC concentrations. Because the attractive van der Waals interactions that promote a parallel orientation[44] compete against repulsive Coulomb interactions that promote an orthogonal orientation[45,46] it is essential to be able to quantify the two contributions accurately. Entropic terms could also be important as it has been shown[47] that packing screw-like rods in a way that their inherent windings interlock minimizes the free energy of the system. Stroobant and co-workers[48] have also

DOI: 10.1021/acs.langmuir.5b00924
Langmuir 2015, 31, 6507−6513

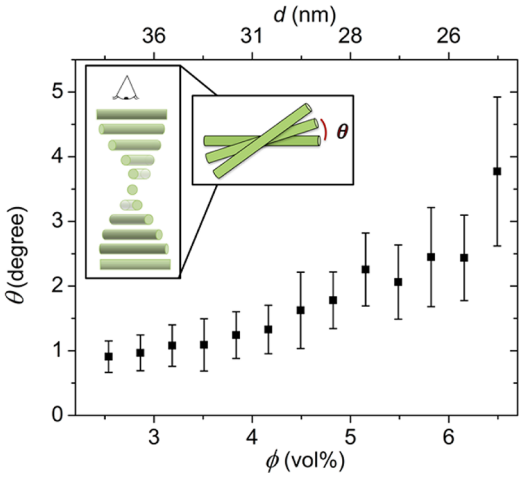

Figure 4. Estimation of the twist angle (θ) as a function of CNC volume fraction (ϕ). The error bars result from Gaussian error propagation of the obtained errors from the pitch and separation distances. The inset is a schematic representation of the helical arranged CNC rods, where in the right image the twist angle is visualized by a simulated top view on the helical arrangement.

shown that a slight twist increases the mobility of the rods and the free volume that results in an entropy increase of the system.

The interaction potential between two rods were calculated using DLVO theory to estimate how the magnitude of the van der Waals attraction and the electrostatic repulsion varies with distance and concentration of two interacting CNC rods.[29,49] Because the CNC dispersions have been dialyzed, it is reasonable to assume that the counterion concentration only consists of protons. Indeed, measurements of the pH show that the pH varies between pH 2.9 and 2.1 at CNC volume fractions ranging between 0.6 and 5.5 vol %, respectively. Within the biphasic region, the pH varies only between pH 2.3 and 2.6, corresponding to an ionic strength of 6 ± 2 mM. Figure 5 shows that the total interaction energy at long center-to-center separation distances (25−50 nm) is essentially zero for crossed cylinders. The interaction energy between parallel cylinders,

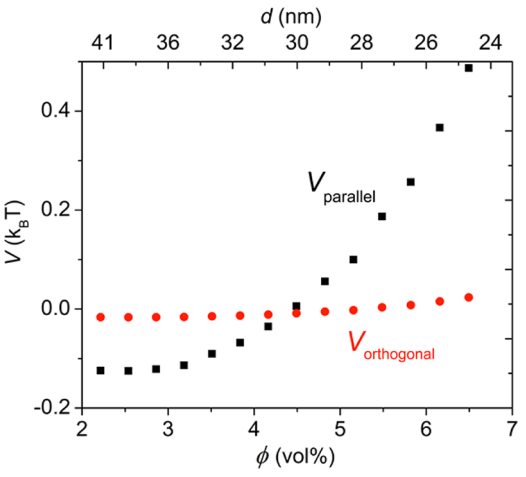

Figure 5. Pair potentials between two interacting cylindrical cellulose nanocrystal rods as a function of center-to-center separation distance d and corresponding CNC volume fraction ϕ for parallel $V_{parallel}$ and orthogonal $V_{orthogonal}$ rod−rod arrangements.

however, is weakly repulsive for center-to-center distances from 24 up to 30 nm, which corresponds to a CNC volume fraction from 6.5 to 4.5 vol %. At longer separation distances, the interaction energy is weakly attractive, suggesting that the electrostatic contribution becomes insignificant. It is important to note that the interparticle attraction is not sufficient to aggregate the CNC rods, even if a larger value for the Hamaker constant is used, as e.g. suggested by Boluk et al.[50] The increase in twist angle with decreasing separation distance, and thus an increasing volume fraction of CNC as obtained from the SAXS data, can be related to the increasing magnitude of the electrostatic repulsion that promotes an increasing deviation from a parallel arrangement. However, more complex interaction models that take into account the intrinsic chirality of the CNC rods and also entropy need to be invoked to describe the rod packing more accurately. Establishing how the rod packing is affected at very high concentrations where the competition between percolation gelation and liquid crystal formation becomes a limiting factor would also give important insight into these systems.[5]

CONCLUSION

The packing of CNC rods in the chiral nematic liquid crystalline phase has been studied as a function of CNC volume fraction using a combination of small-angle X-ray scattering, laser diffraction, and polarized optical microscopy. The average spacing between the CNCs and the pitch of the chiral nematic liquid crystalline phase has been determined at volume fractions ranging from the onset of tactoid formation at 1.6−1.9 vol % up to 6.5 vol %, where the dispersion only contains the anisotropic, chiral nematic phase. The spacing decreases from 51 to 25 nm as the CNC concentration increases from 1.3 to 6.5 vol %, respectively. The pitch decreases from about 15 μm down to 2 μm as the CNC volume fraction increases from 2.5 up to 6.5 vol %. The average twist angle between two neighboring CNC rods was estimated from the volume fraction-dependent pitch and spacing information. We found that the twist angle increases from about 1° up to about 4° as the CNC volume fraction increase from 2.5 to 6.5 vol %. Pair potential estimates using DLVO theory suggest that the electrostatic repulsions increase as the separation distance decreases, thereby promoting a misalignment from the parallel arrangement and increasing the twist angle, in agreement with the experimental results.

ASSOCIATED CONTENT

Supporting Information

More detailed characterization of cellulose nanocrystals including atomic force microscopy, scanning transmission microscopy, and fits of a cylinder and rectangular prism model to determine the form factor; all results listed in a table and a schematic of the laser diffraction measurement setup. The Supporting Information is available free of charge on the ACS Publications website at DOI: 10.1021/acs.langmuir.5b00924.

AUTHOR INFORMATION

Corresponding Author

*E-mail lennart.bergstrom@mmk.su.se (L.B.).

Notes

The authors declare no competing financial interest.

DOI: 10.1021/acs.langmuir.5b00924
Langmuir 2015, 31, 6507−6513

■ ACKNOWLEDGMENTS

The Wallenberg Wood Science Center and the Swedish foundation for strategic research have funded this study.We thank MAX-lab for the provision of beamtime under the proposal 20130343 and the KAW Foundation for the electron microscopy facilities at SU. We also thank Cris Luengo for the MatLab script used to process the AFM images and Ana Labrador for technical assistance at the beamline I911-4.

■ REFERENCES

(1) Hamley, I. W. Liquid Crystal Phase Formation by Biopolymers. *Soft Matter* **2010**, *6*, 1863−1871.
(2) Bouligand, Y. The Renewal of Ideas about Biomineralisations. *C. R. Palevol* **2004**, *3*, 617−628.
(3) Weaver, J. C.; Milliron, G. W.; Miserez, A.; Evans-Lutterodt, K.; Herrera, S.; Gallana, I.; Mershon, W. J.; Swanson, B.; Zavattieri, P.; DiMasi, E.; Kisailus, D. The Stomatopod Dactyl Club: A Formidable Damage-Tolerant Biological Hammer. *Science* **2012**, *336*, 1275−1280.
(4) Al-Sawalmih, A.; Li, C.; Siegel, S.; Fabritius, H.; Yi, S.; Raabe, D.; Fratzl, P.; Paris, O. Microtexture and Chitin/Calcite Orientation Relationship in the Mineralized Exoskeleton of the American Lobster. *Adv. Funct. Mater.* **2008**, *18*, 3307−3314.
(5) Lagerwall, J. P. F.; Schütz, C.; Salajkova, M.; Noh, J.; Hyun Park, J.; Scalia, G.; Bergström, L. Cellulose Nanocrystal-Based Materials: From Liquid Crystal Self-Assembly and Glass Formation to Multifunctional Thin Films. *NPG Asia Mater.* **2014**, *6*, e80.
(6) Marchessault, R. H. .; Morehead, F. F. .; Walter, N. M. Liquid Crystal Systems from Fibrillar Polysaccharides. *Nature* **1959**, *184*, 632−633.
(7) Beck-Candanedo, S.; Roman, M.; Gray, D. G. Effect of Reaction Conditions on the Properties and Behavior of Wood Cellulose Nanocrystal Suspensions. *Biomacromolecules* **2005**, *6*, 1048−1054.
(8) Revol, J.-F.; Godbout, L.; Dong, X.-M.; Gray, D. G.; Chanzy, H.; Maret, G. Chiral Nematic Suspensions of Cellulose Crystallites; Phase Separation and Magnetic Field Orientation. *Liq. Cryst.* **1994**, *16*, 127−134.
(9) Habibi, Y.; Lucia, L. A.; Rojas, O. J. Cellulose Nanocrystals: Chemistry, Self-Assembly, and Applications. *Chem. Rev.* **2010**, *110*, 3479−3500.
(10) Dong, X. M.; Kimura, T.; Revol, J.-F.; Gray, D. G. Effects of Ionic Strength on the Isotropic−Chiral Nematic Phase Transition of Suspensions of Cellulose Crystallites. *Langmuir* **1996**, *12*, 2076−2082.
(11) Dong, X. M.; Gray, D. G. Effect of Counterions on Ordered Phase Formation in Suspensions of Charged Rodlike Cellulose Crystallites. *Langmuir* **1997**, *13*, 2404−2409.
(12) Hirai, A.; Inui, O.; Horii, F.; Tsuji, M. Phase Separation Behavior in Aqueous Suspensions of Bacterial Cellulose Nanocrystals Prepared by Sulfuric Acid Treatment. *Langmuir* **2009**, *25*, 497−502.
(13) Elazzouzi-Hafraoui, S.; Nishiyama, Y.; Putaux, J.-L.; Heux, L.; Dubreuil, F.; Rochas, C. The Shape and Size Distribution of Crystalline Nanoparticles Prepared by Acid Hydrolysis of Native Cellulose. *Biomacromolecules* **2008**, *9*, 57−65.
(14) Shopsowitz, K. E.; Stahl, A.; Hamad, W. Y.; MacLachlan, M. J. Hard Templating of Nanocrystalline Titanium Dioxide with Chiral Nematic Ordering. *Angew. Chem., Int. Ed.* **2012**, *51*, 6886−6890.
(15) Shopsowitz, K. E.; Hamad, W. Y.; MacLachlan, M. J. Chiral Nematic Mesoporous Carbon Derived From Nanocrystalline Cellulose. *Angew. Chem., Int. Ed.* **2011**, *50*, 10991−10995.
(16) Dujardin, E.; Blaseby, M.; Mann, S. Synthesis of Mesoporous Silica by Sol−gel Mineralisation of Cellulose Nanorod Nematic Suspensions. *J. Mater. Chem.* **2003**, *13*, 696−699.
(17) Cheung, C. C. Y.; Giese, M.; Kelly, J. A.; Hamad, W. Y.; Maclachlan, M. J. Iridescent Chiral Nematic Cellulose Nanocrystal/polymer Composites Assembled in Organic Solvents. *ACS Macro Lett.* **2013**, *2*, 1016−1020.
(18) Hyun Park, J.; Noh, J.; Schütz, C.; Salazar-Alvarez, G.; Scalia, G.; Bergström, L.; Lagerwall, J. P. F. Macroscopic Control of Helix Orientation in Films Dried from Cholesteric Liquid-Crystalline Cellulose Nanocrystal Suspensions. *ChemPhysChem* **2014**, *15*, 1477−1484.
(19) Gray, D. G. Chiral Nematic Ordering of Polysaccharides. *Carbohydr. Polym.* **1994**, *25*, 277−284.
(20) Orts, W. J.; Godbout, L.; Marchessault, R. H.; Revol, J.-F. Enhanced Ordering of Liquid Crystalline Suspensions of Cellulose Microfibrils: A Small Angle Neutron Scattering Study. *Macromolecules* **1998**, *31*, 5717−5725.
(21) Ebeling, T.; Paillet, M.; Borsali, R.; Diat, O.; Dufresne, A.; Cavaillé, J.-Y.; Chanzy, H. Shear-Induced Orientation Phenomena in Suspensions of Cellulose Microcrystals, Revealed by Small Angle X-Ray Scattering. *Langmuir* **1999**, *15*, 6123−6126.
(22) Orts, W. J.; Revol, J.-F.; Godbout, L.; Marchessault, R. H. SANS Study of Chirality and Order in Liquid Crystalline Cellulose Suspensions. *MRS Proc.* **1994**, *376*, 317−322.
(23) Moon, R. J.; Martini, A.; Nairn, J.; Simonsen, J.; Youngblood, J. Cellulose Nanomaterials Review: Structure, Properties and Nanocomposites. *Chem. Soc. Rev.* **2011**, *40*, 3941−3994.
(24) Schneider, C. A.; Rasband, W. S.; Eliceiri, K. W. NIH Image to ImageJ: 25 Years of Image Analysis. *Nat. Methods* **2012**, *9*, 671−675.
(25) Labrador, A.; Cerenius, Y.; Svensson, C.; Theodor, K.; Plivelic, T. The Yellow Mini-Hutch for SAXS Experiments at MAX IV Laboratory. *J. Phys. Conf. Ser.* **2013**, *425* (72019), 1−4.
(26) Alina, G.; Butler, P.; Cho, J.; Doucet, M.; Kienzle, P. SANS Analysis software developed under NSF Award DMR, 2009.
(27) Horcas, I.; Fernández, R.; Gómez-Rodríguez, J. M.; Colchero, J.; Gómez-Herrero, J.; Baro, A. M. WSXM: A Software for Scanning Probe Microscopy and a Tool for Nanotechnology. *Rev. Sci. Instrum.* **2007**, *78* (013705), 1−8.
(28) Derjaguin, B.; Landau, L. Theory of the Stability of Strongly Charged Lyophobic Sols and of the Adhesion of Strongly Charged Particles in Solutions of Electrolytes. *Acta Physicochim. URSS* **1941**, *14*, 633−662.
(29) Verwey, E. J. W.; Overbeek, J. T. G. *Theory of the Stability of Lyophobic Colloids*; Elsevier Publishing Co.: New York, 1948.
(30) Israelachvili, J. N. *Intermolecular and Surface Forces*, 2nd ed.; Academic Press: London, 1991.
(31) Stigter, D. Interactions of Highly Charged Colloidal Cylinders with Applications to Double-Stranded DNA. *Biopolymers* **1977**, *16*, 1435−1448.
(32) Sparnaay, M. J. The Interaction between Two Cylinder Shaped Colloidal Particles. *Recl. Trav. Chim. Pays-Bas* **1959**, *78*, 680−709.
(33) Bergström, L.; Stemme, S.; Dahlfors, T.; Arwin, H.; Ödberg, L. Spectroscopic Ellipsometry Characterisation and Estimation of the Hamaker Constant of Cellulose. *Cellulose* **1999**, *6*, 1−13.
(34) Fall, A. B.; Lindström, S. B.; Sundman, O.; Ödberg, L.; Wågberg, L. Colloidal Stability of Aqueous Nanofibrillated Cellulose Dispersions. *Langmuir* **2011**, *27*, 11332−11338.
(35) Beck, S.; Bouchard, J. Auto-Catalyzed Acidic Desulfation of Cellulose Nanocrystals. *Nord. Pulp Pap. Res. J.* **2014**, *29*, 6−14.
(36) Leppänen, K.; Andersson, S.; Torkkeli, M.; Knaapila, M.; Kotelnikova, N.; Serimaa, R. Structure of Cellulose and Microcrystalline Cellulose from Various Wood Species, Cotton and Flax Studied by X-Ray Scattering. *Cellulose* **2009**, *16*, 999−1015.
(37) Jakob, H. F.; Fengel, D.; Tschegg, S. E.; Fratzl, P. The Elementary Cellulose Fibril in Picea Abies: Comparison of Transmission Electron Microscopy, Small-Angle X-Ray Scattering, and Wide-Angle X-Ray Scattering Results. *Macromolecules* **1995**, *28*, 8782−8787.
(38) Revol, J.-F.; Bradford, H.; Giasson, J.; Marchessault, R. H.; Gray, D. G. Helicoidal Self-Ordering of Cellulose Microfibrils in Aqueous Suspension. *Int. J. Biol. Macromol.* **1992**, *14*, 170−172.
(39) Pan, J.; Hamad, W.; Straus, S. K. Parameters Affecting the Chiral Nematic Phase of Nanocrystalline Cellulose Films. *Macromolecules* **2010**, *43*, 3851−3858.
(40) Wensink, H. H.; Jackson, G. Cholesteric Order in Systems of Helical Yukawa Rods. *J. Phys.: Condens. Matter* **2011**, *23*, 194107.

DOI: 10.1021/acs.langmuir.5b00924
Langmuir 2015, 31, 6507−6513

(41) Wensink, H. H.; Jackson, G. Generalized van Der Waals Theory for the Twist Elastic Modulus and Helical Pitch of Cholesterics. *J. Chem. Phys.* **2009**, *130* (234911), 1−15.
(42) Grelet, E.; Fraden, S. What Is the Origin of Chirality in the Cholesteric Phase of Virus Suspensions? *Phys. Rev. Lett.* **2003**, *90*, 198302.
(43) Figgemeier, E.; Hiltrop, K. Quantified Chirality, Molecular Similarity, and Helical Twisting Power in Lyotropic Chiral Nematic guest/Host Systems. *Liq. Cryst.* **1999**, *26*, 1301−1305.
(44) Parsegian, A. V. *Van Der Waals Forces: A Handbook for Biologists, Chemists, Engineers, and Physicists*; Cambridge University Press: New York, 2006.
(45) Brenner, S. L.; Parsegian, V. A. A Physical Method for Deriving the Electrostatic Interaction between Rod-like Polyions at All Mutual Angles. *Biophys. J.* **1974**, *14*, 327−334.
(46) Kornyshev, A. A.; Leikin, S. Electrostatic Interaction between Long, Rigid Helical Macromolecules at All Interaxial Angles. *Phys. Rev. E* **2000**, *62*, 2576−2596.
(47) Straley, J. P. Theory of Piezoelectricity in Nematic Liquid Crystals, and of the Cholesteric Ordering. *Phys. Rev. A* **1976**, *14*, 1835−1841.
(48) Stroobants, A.; Lekkerkerker, H. N. W.; Odijk, T. Effect of Electrostatic Interaction on the Liquid Crystal Phase Transition in Solutions of Rodlike Polyelectrolytes. *Macromolecules* **1986**, *19*, 2232−2238.
(49) Derjaguin, B.; Landau, L. Theory of the Stability of Strongly Charged Lyophobic Sols and of the Adhesion of Strongly Charged Particles in Solutions of Electrolytes. *Prog. Surf. Sci.* **1993**, *43*, 30−59.
(50) Boluk, Y.; Zhao, L.; Incani, V. Dispersions of Nanocrystalline Cellulose in Aqueous Polymer Solutions: Structure Formation of Colloidal Rods. *Langmuir* **2012**, *28*, 6114−6123.

DOI: 10.1021/acs.langmuir.5b00924
Langmuir 2015, 31, 6507−6513